Elementary approach on the prediction of next material composition using AI technology:

Improvement of characteristic by changing two components

Daisuke Tanaka (Department of Mechanical Engineering, National Institute of Technology (KOSEN), Niihama College, d.tanaka@niihama-nct.ac.jp)
Susumu Nakayama (Department of Applied Chemistry and Biotechnology, National Institute of Technology (KOSEN), Niihama College, s.nakayama@niihama-nct.ac.jp)

Abstract

This study aims to identify the factors affecting the characteristics of samples, such as photoluminescence intensities, and identify the relationship between performance improvement and the search parameters for material composition. Subsequently, we optimize the experimental conditions to provide the maximum characteristic value. First, the process parameters are introduced as input values to the artificial intelligence (AI)-based model; then, we obtain a generalized equation to establish relationship between the characteristics of the samples and the process parameters. Subsequently, the new samples suitable for determining an accurate model and optimizing the process parameters are calculated and recommended to the user. Finally, the obtained formula is optimized, and the optimum values for achieving maximum characteristic are determined. Experimental validation using the AI program developed in this study found that the two components (x, y) that provide the strongest PL intensity in the $Sr_x(La10_{-x-y}Eu_y)(SiO_4)_6O_{3-x/2}$ (x=2–6, y=0.6–1.2) red-emitting phosphors can be easily estimated from approximately 10 initial data points.

Key words

artificial intelligence, haze optimization, material search, ceramics, photoluminescence

1. Introduction

Nowadays, the development of materials using artificial intelligence technology is being actively implemented; moreover, the effectiveness of this method has been widely demonstrated in the literature. Material Informatics (MI) is the cross-disciplinary field that combines material science and artificial intelligence, which has been adopted across the industrial world. Machine learning methods, especially Bayesian optimization (BO) methods, are widely used in the field of MI. The BO method can be regarded as an experimental design method. In recent years, several studies have reported the effectiveness of BO methods. For example, Sakurai et al. (2019) found aperiodic multilayered metamaterials exhibiting high and sharp emissivity from over 8 billion candidates. The BO method reduces the calculation cost of electromagnetic simulations to 168 million patterns (which is approximately 2% of the total patterns needed). Hou et al. (2019) also reported the discovery of an optimal composition of aluminum, iron, and silicon for thermoelectric properties in a mid-temperature range with the assistance of BO methods. Sumita et al. (2018) solved the problem wherein the ordinal AI model automatically designs deviating structures of organic molecules (i.e., the structures that do not exist in nature). The structures designed by the new AI model were chemically stable and exhibited desired properties. Further, Shimizu et al. (2020) developed a robot system that autonomously searches for new materials by combining machines that iteratively perform machine learning and experimental operations; they successfully minimized the electrical resistance of titanium dioxide thin films. Their proposed system achieved 10-fold experimental efficiency relative to the conventional method; moreover, it led to the development of a fully automated and autonomous research style in which robot systems and humans collaborate. However, it is assumed that applying AI methods to a new field could be difficult for non-specialists in AI technology. In this study, we develop an open-access web application that enables non-specialists of AI in the material science field to use BO methods. The application provides the next set of experimental conditions to find the optimal structure of chemical combinations from user input, such as the current experimental conditions and corresponding evaluations (e.g., intensity, emissivity, and calorific value). This report demonstrates the effectiveness of the application basis the simulation results obtained from actual experimental data.

2. Methodology and materials

2.1 Bayesian optimization

Bayesian optimization is a commonly used method to obtain the optimal input that maximizes a function. This problem can be expressed as follows:

$$\max_x f(x).$$

The input $x \in R^d$ is a combination of d values for an experimental setting, and the objective function $f(x)$ is an unknown continuous function. For example, in the development of luminescent materials, the values involved in the composition would be x, and the resulting intensity of the material would

be $f(x)$. However, the relationship between the composition and the intensity is difficult to express explicitly in mathematical form. Therefore, we find the relationship $f(x)$ from the experimental data.

We model the function $f(x)$ using Gaussian process regression. This method enables us to predict the output uncertainty. The top panel in Figure 1 shows an example of the Gaussian process regression model with one-dimensional input x. The experimental data (x_k, $f(x_k)$) used to obtain this model are (0.1, –0.1), (0.2, 0.3), and (0.8, –0.1), which are indicated by filled circles. The solid line indicates the predictive mean (regarded as the predicted value of $f(x)$), and the gray-colored area indicates the predictive variance, which implies the uncertainty of the prediction. As the experimental data are not obtained at around x=0.5 and x>0.8, the uncertainty is relatively larger in the results. Note that the objective here is to obtain the optimal input that maximizes the function. Therefore, exploration and exploitation are required in experiments. In the former, we obtain data for the construction of a more exact model, which is achieved by obtaining the data at the input around the larger uncertainty. For the latter, we obtain the data for finding the optimal input, which is achieved by obtaining the data at the input around the larger predictive mean. This implies the presence of a tradeoff between exploration and exploitation. To address this tradeoff, a function called the acquisition function is used to propose the next experimental condition. An example of the acquisition function is illustrated in the bottom panel of Figure 1. The function is calculated using the predictive mean and the uncertainty; the results confirm that the function is maximized at x=0.5, which is the point with the larger function value and the larger uncertainty. Thus, the framework for iteratively modeling using Gaussian process regression and conducting experiments under the proposed conditions is called Bayesian optimization (BO). As the acquisition function, the expected improvement (EI) is calculated using the predictive mean; in general, uncertainty is used. In this study, we used the modified EI to obtain two or more experimental conditions. The modification involved penalizing the acquisition function by the distance of the inputs between the proposed (next) input and the newly proposed (after next) input (see for a detailed explanation of Bayesian optimization (Frazier, 2018).

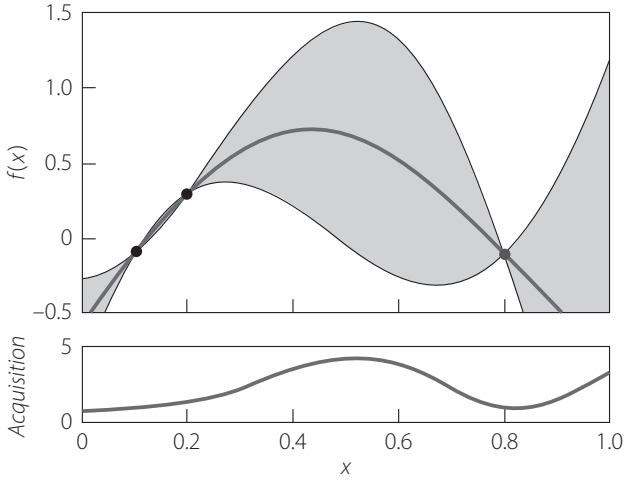

Figure 1: Example of Bayesian optimization

Notes: Top panel: an example of the Gaussian process regression model with one-dimensional input x. Bottom panel: an example of the acquisition function. The experimental data (x_k, $f(x_k)$) used to obtain this model are (0.1, –0.1), (0.2, 0.3), and (0.8, –0.1), indicated by the large dots in the figure. The solid line indicates the predictive mean (regarded as the predicted value of $f(x)$, while the gray-colored area shows the predictive variance, which indicates the uncertainty of the prediction. The next experimental condition (x) is determined using the acquisition function.

2.2 Experimental procedure

In this work, numerical simulations were performed using actual experimental data through the use of a red-emitting phosphor $Sr_x(La_{10-x-y}Eu_y)(SiO_4)_6O_{3-x/2}$ (x=2–6, y=0.6–1.2) (Nakayama, 2019) with a system program, wherein two components in the material were changed. The preparation methodology and evaluation of the phosphor are as follows. $Sr_x(La_{10-x-y}Euy)(SiO_4)_6O_{3-x/2}$ was prepared from $SrCO_3$ (99.9 % purity, Fujifilm Wako Pure Chemical Co.), La_2O_3 (99.9 % purity, Shin-Etsu Chemical Co., Ltd.), and Eu_2O_3 (99.9 % purity, Shin-Etsu Chemical Co., Ltd.) powders. These component powders were mixed using a ball mill (Fritsch Co., Pulverisette 6). After drying, the powders were pressed into discs under a pressure of 100 MPa and sintered at 1500 °C for 2 h in air. The sintered disks were crushed with a zirconia mortar to obtain powders for various measurements. The obtained phosphors were characterized by X-ray diffraction and fluorescence spectroscopy. X-ray diffraction data were obtained using an X-ray diffractometer (MiniFlex II, Rigaku Co.). Emission spectra were measured on a spectrofluorometer FP-6500 (JASCO Co.) with an excitation wavelength of 395 nm. The strongest emission spectrum peak was observed at approximately 614 nm.

3. Experimental and optimization results (verification of prediction of optimal composition by AI)

The results of the X-ray diffraction analysis revealed the $Sr_x(La_{10-x-y}Eu_y)(SiO_4)_6O_{3-x/2}$ (x=2–6, y=0.6–1.2) samples to be composed of a single phase of the oxy-apatite structure. The region of x=2–6 is called the apatite composition. The excitation (with emission wavelength λ_{em}=618 nm) and emission (with excitation wavelength λ_{ex}=395 nm) spectra of the $Sr_{4.5}(La_{4.4}Eu_{1.1})(SiO_4)_6O_{0.75}$ phosphor sample are shown in Figure 2. Figure 3 shows the PL intensities (a. u.) of the $Sr_x(La_{10-x-y}Eu_y)(SiO_4)_6O_{3-x/2}$ (x=2–6, y=0.6–1.2) red-emitting phosphors at around 614 nm for excitation wavelength of 395 nm. The nine underlined bold values of PL intensity in Figure 3 are the initial input data to the AI program. For calculation, the con-

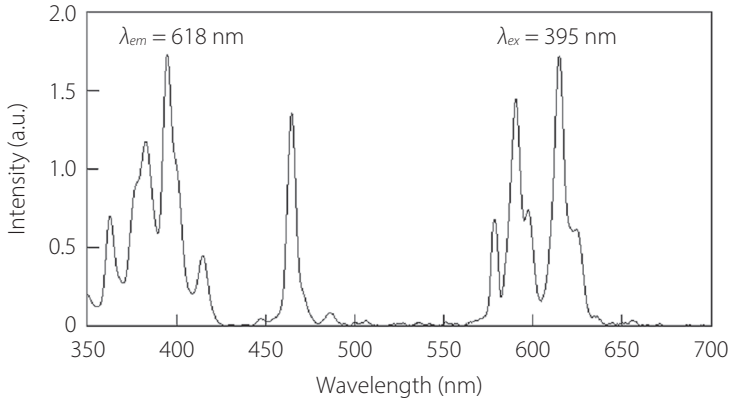

Figure 2: Excitation and emission spectra of $Sr_{4.5}(La_{4.4}Eu_{1.1})(SiO_4)_6O_{0.75}$ phosphor sample

figurations were as follows; *x* was 0.5 intervals in the range of 2.0–6.0, *y* was 0.1 intervals in the range of 0.4–1.4, and the next candidate composition was one. Although the values at (*x*=2.0, *y*=0.8), (*x*=3.0, *y*=0.8), (*x*=4.0, *y*=0.8), (*x*=5.0, *y*=0.8), and (*x*=6.0, *y*=0.8) in the previous report (Nakayama, 2019) were used as input data, the next candidate composition could not be obtained under the aforementioned conditions. Then, as a result of sequentially adding the data from preliminary experiments conducted at (*x*=3.0, *y*=0.6), (*x*=3.0, *y*=1.2), (*x*=3.0, *y*=1.4), and (*x*=4.0, *y*=1.0), the next candidate (*x*=3.0, *y*=1.0) was obtained. Subsequently, candidates (*x*=3.0, *y*=1.0), (*x*=4.5, *y*=1.1), (*x*=5.0, *y*=1.1), and (*x*=4.5, *y*=1.1) were obtained; the fifth candidate was again the same as the composition (x = 4.5, *y*=1.1) of the highest PL intensity (1.72). The results are depicted in Figure 4. Thus, the AI calculation process was terminated. Next, the number of next candidates was set to two, and the calculations were performed. Candidates {(*x*=3.0, *y*=1.0) and (*x*=3.5, *y*=0.9)}, {(*x*=4.5, *y*=1.1) and (*x*=3.0, *y*=0.8)}, {(*x*=5.0, *y*=1.1) and (*x*=3.5, *y*=0.9)}, {(*x*=4.0, *y*=1.1) and (*x*=3.5, *y*=0.9)}, {(*x*=4.5, *y*=1.1) and (*x*=3.5, *y*=0.9)}, and {(*x*=4.5, *y*=1.1)

y \ *x*	2.0	2.5	3.0	3.5	4.0	4.5	5.0	5.5	6.0
1.4			**0.39**						
1.3						*1.21*			
1.2			**1.36**		*1.36*	*1.65*	*1.42*		
1.1				*1.41*	(1)1.47 (2)1.47	(1)1.72 (2)1.72	(1)1.49 (2)1.49	*1.39*	
1.0			(1)1.39 (2)1.39		**1.65** (2)1.65	*1.67*	*1.63*		*1.21*
0.9				(2)1.40	(2)1.48	*1.50*			
0.8	**1.22**		**1.38** (2)1.38		**1.21**		**1.18**		**0.75**
0.7									
0.6			**1.04**						
0.5									
0.4									

Figure 3: PL intensities (a.u.) at around 614 nm (excitation: 395 nm) for the composition (*x*, *y*) of $Sr_x(La_{10-x-y}Eu_y)(SiO_4)_6O_{3-x/2}$ phosphor

Notes: The underlined bold values indicate the initial input data to the AI program. The values of (1) are the data when the next candidate is set to one. The values of (2) are the data where the next candidate is set to two. The values in italics refer to other data.

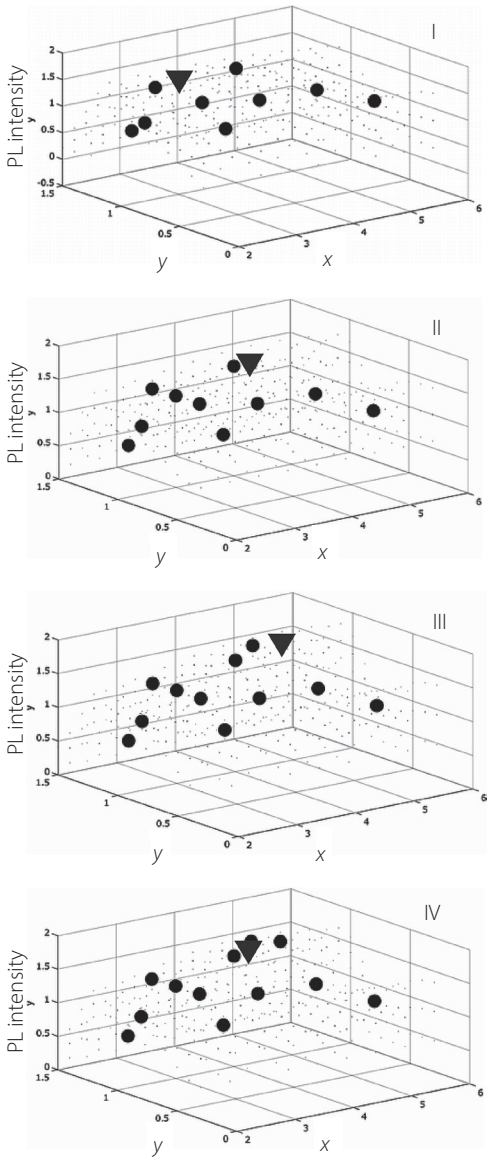

Figure 4: Results of AI calculation processing when the subsequent candidate is set to one

Notes: The nine compositions at (x=2.0, y=0.8), (x=3.0, y=0.8), (x=4.0, y=0.8), (x=5.0, y=0.8), (x=6.0, y=0.8), (x=3.0, y=0.6), (x=3.0, y=1.2), (x=3.0, y=1.4), and (x=4.0, y=1.0) are the initial input data for the AI program. The triangular points in each figure represent the latest candidate composition (x, y) and evaluated PL intensity, as sequenced by the corresponding coordinates. I: (x=3.0, y=1.0), II: (x=4.5, y=1.1), III: (x=5.0, y=1.1), and IV: (x=4.5, y=1.1). The dots in the figures denote the initial input data and the triangular points from immediately preceding figure.

and (x=4.0, y=1.0)} were obtained. The calculation was terminated as the same candidate composition was obtained in successive iterations. The results are summarized in Figure 5. Additional experiments were performed on the 10 compositions around the composition (x=4.5, y=1.1), where the highest PL intensity was obtained, but none exceeding the PL intensity at (x=4.5, y=1.1) was observed. From the above results, we conjecture that the composition with the highest PL intensity can be obtained by repeating the process of ob-

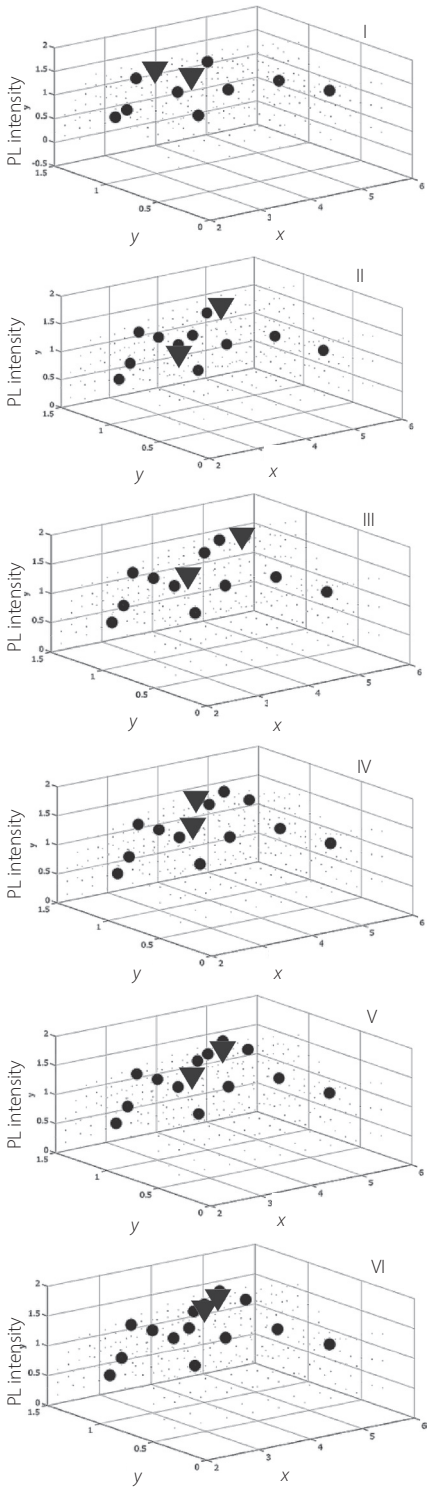

Figure 5: Results of AI calculation processing when the subsequent candidate is set to two

Notes: The nine compositions at (x=2.0, y=0.8), (x=3.0, y=0.8), (x=4.0, y=0.8), (x=5.0, y=0.8), (x=6.0, y=0.8), (x=3.0, y=0.6), (x=3.0, y=1.2), (x=3.0, y=1.4), and (x=4.0, y=1.0) are the initial input data for the AI program. The triangular points in each figure denote the latest candidate composition (x, y) and evaluated PL intensity, as sequenced by the corresponding coordinates. I: {(x=3.0, y=1.0) and (x=3.5, y=0.9)}, II: {(x=4.5, y=1.1) and (x=3.0, y=0.8)}, III: {(x=5.0, y=1.1) and (x=3.5, y=0.9)}, IV: {(x=4.0, y=1.1) and (x=3.5, y=0.9)}, V: {(x=4.5, y=1.1) and (x=3.5, y=0.9)}, and VI: {(x=4.5, y=1.1) and (x=4.0, y=1.0)}. The dots in the figures denote the initial input data and the triangular points from immediately preceding figure.

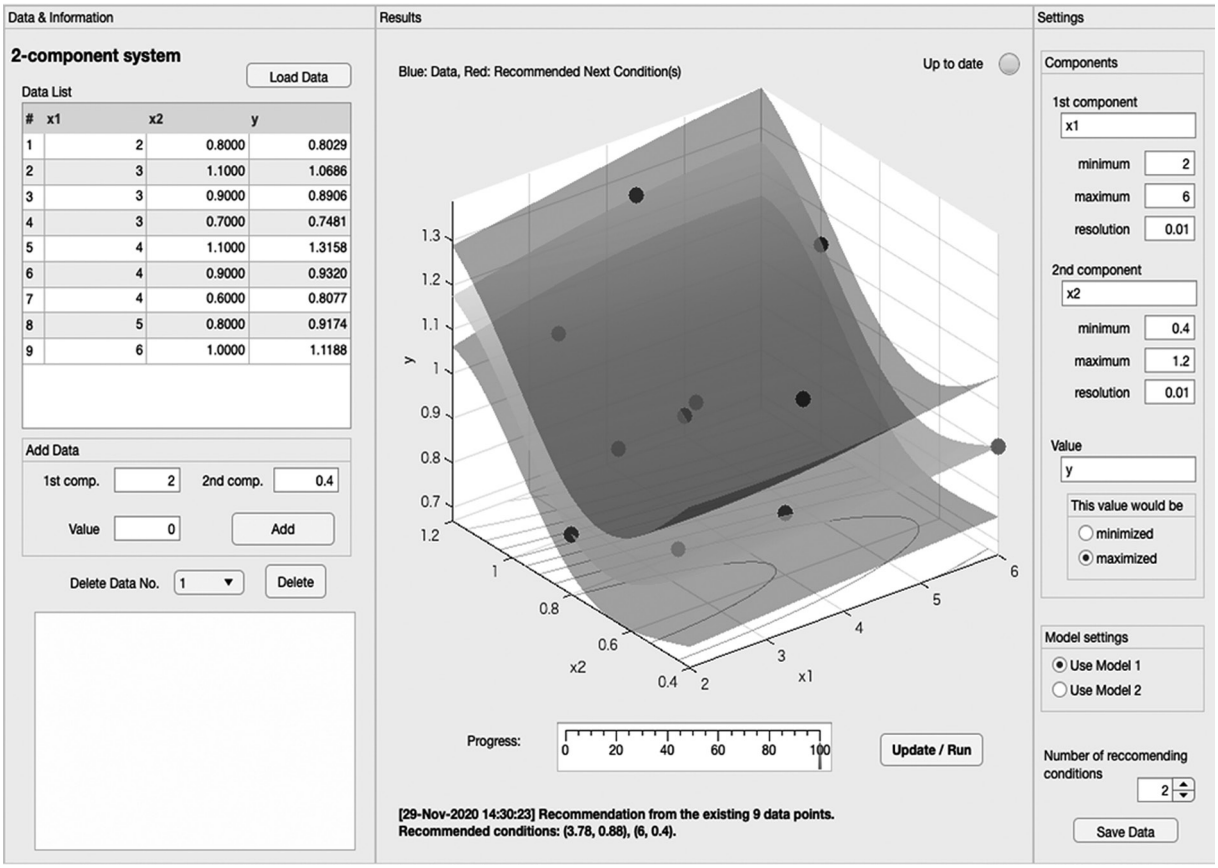

Figure 6: Screenshot of the proposed application

Notes: In the panel on the left side of this figure, the experimental data are shown in the table, and the data may be edited on the table. Moreover, this panel enables the addition or deletion of data. The panel on the right has settings that can be customized to obtain new experimental data, while the central panel show the model obtained from the experimental data and recommended conditions. Refer to https://www.daisuket.net/bo/index.html for further details.

taining the next candidate from the nine initial data, adding the data, and performing the calculation approximately five times. Therefore, to achieve the target characteristics from a limited number of experiments, the AI program that provides the next candidate composition developed in this study can be regarded as effective in a system with two component changes.

4. Conclusion

In this study, we performed a numerical simulation using actual experimental data in a system with two component changes. It was suggested that the next formulation candidates could be obtained from several experimental data and that a formulation with the expected characteristics could be obtained as the experiment was further advanced. The AI program created in this report will be open (https://www.daisuket.net/bo/index.html) to facilitate collaboration between researchers and engineers across different fields. Figure 6 presents the user interface of the proposed application. An advantage of our program is that it can directly be used on web browsers without (any prior installation requirements). It will soon be made available for tablets. For our future work, we are considering systems that modify three or more components. The validation of this method in other fields will also be explored our future work.

Acknowledgement

We would like to thank the Grant of Daiichi Kigenso Kagaku Kogyo Co. Ltd. and Editage (www.editage.com) for English language editing.

References

Frazier, P. I. (2018). A tutorial on bayesian optimization. arXiv:1807.02811.

Hou, Z., Takagiwa, Y., Shinohara, Y., Xu, Y., and Tsuda, K. (2019). Machine-learning-assisted development and theoretical consideration for the $Al_2Fe_3Si_3$ thermoelectric material. *ACS Applied Materials & Interfaces*, Vol. 11, 11545-11554.

Nakayama, S. (2019). Red-light emission characteristics of $Sr_x(La_{9.2-x}Eu_{0.8})(SiO_4)_6O_{3-x/2}$ (x=2–6) oxy-apatite phosphors. *Optik*, Vol. 182, 944-948.

Sakurai, A., Yada, K., Simomura, T., Kashiwagi, S. Ju, M., Okada, H., Nagao, T., Tsuda, K., and Shiom, J. (2019). Ultranarrow-band wavelength-selective thermal emission with aperiodic mul-

tilayered metamaterials designed by Bayesian optimization. *ACS Central Science*, Vol. 5, 319-326.

Shimizu, R., Kobayashi, S., Watanabe, Y., Ando, Y., and Hitosugi, T. (2020). Autonomous materials synthesis by machine learning and robotics. *APL Materials*, Vol. 8, 111110.

Sumita, M., Yang, X., Ishihara, S., Tamura, R., and Tsuda, K. (2018). Hunting for organic molecules with artificial intelligence: Molecules optimized for desired excitation energies. *ACS Central Science*, Vol. 4, 1126-1133.

(Received: April 29, 2021; Accepted: May 21, 2021)